# Supersolid striped droplets in a Raman spin-orbit-coupled system

J. Sánchez-Baena,* J. Boronat,† and F. Mazzanti‡
*Departament de Física, Universitat Politècnica de Catalunya, Campus Nord B4-B5, 08034 Barcelona, Spain*

(Received 7 July 2020; accepted 22 October 2020; published 9 November 2020)

We analyze the role played by quantum fluctuations on a Raman spin-orbit-coupled system in the stripe phase under attractive interspin interactions. We show that beyond-mean-field effects stabilize the collapse predicted by mean-field theory for attractive enough interspin interactions and induce the emergence of two phases, a gas and a liquid, which also show spatial periodicity along a privileged direction. We show that the energetically favored phase is determined by the Raman coupling and the spin-dependent scattering lengths. We obtain the ground-state solution of the finite system by solving the extended Gross-Pitaevskii equation and find self-bound dropletlike solutions that feature internal structure through a striped pattern. We estimate the critical binding number of these droplets and show that their value is experimentally accessible. We report an approximate energy functional in order to ease the evaluation of the Lee-Huang-Yang correction in practical terms.

DOI: 10.1103/PhysRevA.102.053308

## I. INTRODUCTION

Spin-orbit coupling (SOC), which is the interplay between a particle's momentum and its spin, has been a subject of interest in recent years, both theoretically and experimentally. It plays an important role in a wide variety of exotic quantum phenomena, such as topological insulators [1] and topological superconductors [2]. Spin-orbit coupling is a relativistic effect naturally found in electronic and atomic systems. However, it can also be synthetically engineered [3] in ultracold atomic gases, which represent an excellent platform to study the physics of SOC due to their high controllability and tunability. In particular, Raman SOC was first implemented experimentally by inducing a Raman coupling via two laser beams on an atomic $\Lambda$-type configuration [4,5]. Raman SOC has been realized with $^{87}$Rb atoms, both in the continuum [4] and in a lattice [6,7], and with other atomic species such as $^{6}$Li [8] and $^{40}$K [9]. In this context, two hyperfine states of an atom are labeled as pseudospin states, although alternative schemes using other types of states as pseudospins have been realized. As an example, the two lowest eigenstates of an asymmetric double well in a superlattice have also been employed as pseudospins [10].

In this work we focus on Raman SOC, which couples the linear momentum of an atom with its spin according to

$$\hat{W}^{\mathrm{SOC}} = \frac{\hbar k_0}{m}\hat{P}_x\hat{\sigma}_z + \frac{\hbar^2 k_0^2}{2m} - \frac{\Omega}{2}\hat{\sigma}_x, \tag{1}$$

with $m$ the atomic mass, $\hat{P}_x$ the $x$ component of the momentum operator, $\hat{\sigma}_x$ and $\hat{\sigma}_z$ the Pauli matrices, $\Omega$ the Raman coupling, and $k_0$ the magnitude of the wave vector difference between the two laser beams. We are particularly interested in the emergence of a stripe phase, which arises from the breaking of two symmetries: a gauge symmetry, giving rise to off-diagonal long-range order, and spatial symmetry, seen as a periodic density modulation in space [11]. In contrast to other systems featuring spatial ordering like dipoles [12,13], this property is present in SOC systems even in ultradilute conditions, mainly because of the different physical mechanism that gives rise to stripes: While in dipolar systems it corresponds to the anisotropy of the dipolar interaction, in SOC systems stripes are induced by the momentum degeneracy of the dispersion relation induced by SOC. The stripe phase has been both predicted theoretically [5,11] and detected experimentally [10] and the resulting stripes have been shown to be superfluid [11,14,15], and thus often referred to as supersolid stripes or superstripes. It has also been shown that the increase of interatomic correlations enhances the domain of the stripe phase in the phase diagram of Raman SOC systems [15].

As it happens in ultradilute Bose-Bose mixtures, systems with spin-dependent interactions can become unstable at the mean-field level for some values of the spin-dependent scattering lengths. A well-known result for unstable Bose-Bose mixtures is that quantum fluctuations can stabilize the system through the Lee-Huang-Yang (LHY) energy correction, giving rise to liquid droplets [16], which have been realized in experiments using $^{39}$K atoms [17,18]. In this work we investigate if the same mechanism also holds in a system under Raman SOC in the stripe phase. While in previous works beyond mean-field properties like the excitation spectrum and the static structure factor of the stripe phase have been reported [11], the complete LHY energy correction containing SOC terms has not been derived. We evaluate this term in order to estimate the role played by quantum fluctuations in a stripe state under Raman SOC which is unstable at the mean-field level.

At this point it is interesting to remark that, to date, available experiments incorporating Raman SOC effects are restricted to repulsive inter- and intraspin interactions, thus

*juan.sanchez.baena@upc.edu
†jordi.boronat@upc.edu
‡ferran.mazzanti@upc.edu

 

avoiding mean-field collapse. These systems can be accurately described with the mean-field approximation [5], at least for low gas parameter values up to $na_{+1,+1}^3 \sim 10^{-4}$ [15], with $n$ the density and $a_{+1,+1}$ the spin-up–spin-up scattering length. However, state-of-the-art experiments currently under development, featuring attractive interspin interactions, are pursuing the observation of droplet formation in a Raman SOC system.

This paper is organized as follows. In Sec. II we present the Hamiltonian and the length and energy scales of the reduced units employed. In Sec. III we present the main results of this work. We briefly review the Bogoliubov–de Gennes formalism in Sec. III A. We present the phase diagram of the system stabilized by quantum fluctuations in Sec. III B, while self-bound striped droplet formation and the resolution of the extended Gross-Pitaevskii equation are discussed in Sec. III C. In Sec. IV we summarize the main conclusions of our work.

## II. HAMILTONIAN

We study an $N$-particle system governed by the Hamiltonian

$$\hat{H} = \sum_i \left( \frac{\hat{P}_i^2}{2m} + \hat{W}_i^{\mathrm{SOC}} \right) + \sum_{i<j} \hat{V}_{ij} = \sum_i \hat{H}_{0,i} + \sum_{i<j} \hat{V}_{ij}, \tag{2}$$

with $\hat{V}_{ij}$ a two-body spin-dependent pseudopotential given by

$$\hat{V}_{ij} = \sum_{s_1,s_2} g_{s_1,s_2} \delta(\vec{r}_i - \vec{r}_j) |s_1, s_2\rangle\langle s_1, s_2|, \tag{3}$$

with $g_{s_1,s_2} = \frac{4\pi\hbar^2 a_{s_1,s_2}}{m}$, $s_i$ the spin coordinate of the $i$ th particle, and $a_{s_1,s_2}$ the spin-dependent scattering lengths. To reduce the number of variables, we set $a \equiv a_{+1,+1} = a_{-1,-1} \neq a_{+1,-1} = a_{-1,+1}$. We introduce the parameter $\gamma = (a - a_{+1,-1})/(a + a_{+1,-1})$, which measures the relative strength of the interaction in the different spin channels. Throughout this work, all quantities are given in reduced units defined by the length and energy scales given by $a_0 = 1/k_0$ and $\varepsilon_0 = \hbar^2 k_0^2/2m$, respectively.

## III. QUANTUM FLUCTUATIONS IN A RAMAN SOC SYSTEM IN THE STRIPE PHASE

### A. Bogoliubov–de Gennes formalism

In second quantization, the system can be described by the field operator spinor, $\hat{\Psi}(\vec{r}) = [\hat{\psi}^{+1}(\vec{r})\hat{\psi}^{-1}(\vec{r})]^\tau$, with the $+1$ ($-1$) index denoting the up-spin (down-spin) component. The dynamics of the field operator are governed by the Heisenberg equation [19]

$$i\frac{d\hat{\Psi}(t)}{dt} = \hat{H}_0\hat{\Psi} + \left( \frac{2G_1}{n}\hat{\Psi}^\dagger\hat{\Psi} + \frac{2G_2}{n}(\hat{\Psi}^\dagger\hat{\sigma}_z\hat{\Psi})\hat{\sigma}_z \right)\hat{\Psi}, \tag{4}$$

with $G_1 = n(g_{+1,+1} + g_{+1,-1})/4$ and $G_2 = n(g_{+1,+1} - g_{+1,-1})/4$. In the stripe phase, the condensate wave function can be written as [11,20]

$$\vec{\psi}_0(\vec{r}) = \frac{1}{\sqrt{\tilde{V}}} \sum_{n\in\mathbb{Z}} \vec{\psi}_{0,n} e^{ik_1 x + 2ink_1 x}, \tag{5}$$

with $\tilde{V} = Va_0^3$ the dimensionless volume of the system and the amplitudes fulfilling the condition $\psi_{0,j}^{\pm 1} = (\psi_{0,-j-1}^{\mp 1})^*$ [20]. The value of $\vec{\psi}_{0,n}$ and the stripe momentum $k_1$ can be obtained by minimizing the mean-field energy. We do that using the simulated-annealing algorithm [21]. The effect of quantum fluctuations can be included following the Bogoliubov scheme, where the time-dependent field operator is written as

$$\hat{\Psi}(t) = e^{-i\mu t}[\hat{\psi}_0 + \delta\hat{\Psi}(t)], \tag{6}$$

with $\hat{\psi}_0 = \vec{\psi}_0(\vec{r})\hat{a}_0$ corresponding to the condensate state and $\delta\hat{\Psi}(t)$ accounting for the quantum fluctuations. For the stripe phase, $\delta\hat{\Psi}(t)$ can be decomposed as [20]

$$\begin{aligned}\delta\hat{\Psi}(\vec{r},t) = &\sum_{\substack{0<k_x<k_1 \\ 0<k_y,k_z<\infty \\ l}} \vec{f}_{\vec{k}_1+\vec{k},l}(\vec{k},\vec{r})e^{-iE_{\vec{k}_1+\vec{k},l}t}\hat{b}_{\vec{k}_1+\vec{k},l} \\ &+ \vec{f}^*_{\vec{k}_1-\vec{k},l}(\vec{k},\vec{r})e^{iE_{\vec{k}_1-\vec{k},l}t}\hat{b}^\dagger_{\vec{k}_1-\vec{k},l} \\ &+ \vec{g}_{\vec{k}_1-\vec{k},l}(\vec{k},\vec{r})e^{-iE_{\vec{k}_1-\vec{k},l}t}\hat{b}_{\vec{k}_1-\vec{k},l} \\ &+ \vec{g}^*_{\vec{k}_1+\vec{k},l}(\vec{k},\vec{r})e^{iE_{\vec{k}_1+\vec{k},l}t}\hat{b}^\dagger_{\vec{k}_1+\vec{k},l},\end{aligned} \tag{7}$$

with $\vec{k}_1 = k_1\vec{e}_x$ and $\vec{e}_x$ the unitary vector along the $x$ axis. Notice that, in this expression, the momentum runs over all possible values in the first Brillouin zone ($0 < k_x < 2k_1$ and $0 < k_y, k_z < \infty$). The excitation spectrum and the Bogoliubov amplitudes are obtained by substituting Eqs. (6) and (7) into Eq. (4) and solving a diagonalization problem. This can be done by expanding the amplitudes of Eq. (7) in Bloch waves [11]. Once this is done with the Bogoliubov amplitudes, one can numerically calculate the LHY energy correction. Since the condensate state presents periodic density modulations on the $x$ axis, the LHY integral implies a sum running over all Brillouin zones. In practice, though, we truncate the sum and keep only a finite number of terms. Additional approximations described in Appendix A must be adopted in order to keep the computational cost of the calculation down to a reasonable level, since the size of the aforementioned diagonalization problem scales with the number of Brillouin zones in the integration.

As happens in other non-SOC systems, the LHY integral is ultraviolet divergent and must be regularized. By computing it over increasingly larger cylindrical domains, we find that its divergent behavior equals that of the function $I_\eta(V_I) = I_0 + \int_{V_I} d\vec{k}\,\eta/k^2$, with $V_I$ the integration volume and $\eta$ and $I_0$ fitting parameters. We use dimensional regularization [22,23] to regularize this integral (see Appendix B). We also discuss the convergence of the regularized integral with respect to the number of discretization points in momentum space and the number of Brillouin zones in Appendix C.

### B. Phase diagram

We are particularly interested in the role played by quantum fluctuations when the mean-field system is unstable. Using the expression for the mean-field energy per particle of Ref. [5] together with $\frac{\partial^2 E}{\partial V^2}$, it can be shown that the mean-field stripe state is unstable for $G_1 < 0$ if $2 > |G_1|$ in reduced units, a requirement fulfilled in all our calculations. Under

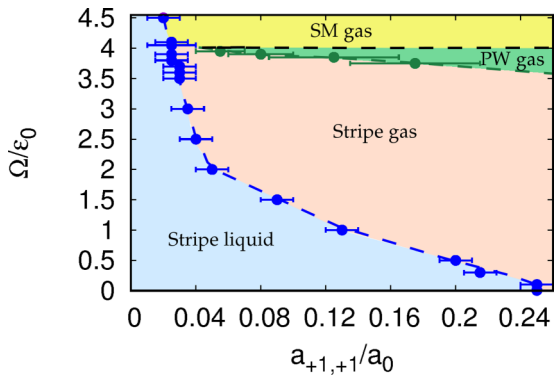


FIG. 1. Phase diagram of the system stabilized by quantum fluctuations at the LHY level for the different stripe phases with $\gamma = -21$.

these conditions, the LHY energy is positive and stabilizes the collapsing mean-field state. This is similar to the result obtained for unstable Bose-Bose mixtures without SOC [16], although remarkable differences exist between the two cases, as detailed below.

The phase diagram of the stabilized system, as a function of $\Omega$ and $a_{+1,+1} > 0$, for $\gamma = -21$ (i.e., $a_{+1,-1} = -1.1a_{+1,+1}$) is shown in Fig. 1. The phase diagram includes beyond-mean-field effects, with the ground state being the phase of minimum energy. Error bars account for the numerical error associated with the finite number of Brillouin zones and integration points considered in the calculations. As it can be seen from the figure, depending on the value of the Raman coupling $\Omega$ and the scattering lengths, the homogeneous system can be either a liquid ($n^{(0)} \neq 0$, with $n^{(0)}$ the density for which $E/N$ is minimum) or a gas (for which $\frac{dE/N}{dn} > 0 \forall n$). Therefore, in order to determine if the system is in a liquid or in a gas state, we compute $E/N$ for different densities for fixed $\{\Omega, a_{+1,+1}\}$. Typically, $n \in [3.78 \times 10^{-4}, 4.93 \times 10^{-3}]$, although this range is extended in some cases up to $n \simeq 0.1$. We report in Fig. 2 the rescaled mean field and mean field plus LHY energies per particle as a function of the density for two different points of the phase diagram that correspond to the stripe liquid and stripe gas phases, respectively. The liquid-gas transition is an effect entirely induced by the presence of the SOC interaction, since for unstable Bose-Bose mixtures without SOC the stabilization of the collapse by the LHY energy always brings the homogeneous system to a liquid state [16].

Figure 1 indicates that increasing the Raman coupling in the stripe phase leads to a lower interval of scattering lengths where the system is in the liquid phase. In this way, for fixed $a_{+1,+1}$, increasing $\Omega$ leads to a decrease in $n^{(0)}$, leading to a less correlated liquid. In much the same way, increasing $a_{+1,+1}$ with $\gamma = -21$ and keeping $\Omega$ constant drives the system from a liquid state to a gas, i.e., the equilibrium density $n^{(0)}$ shifts to lower values until $n^{(0)} = 0$, with the gas parameter $n^{(0)}a^3_{+1,+1}$ also decreasing. Remarkably, this behavior is not seen in ultradilute non-SOC Bose-Bose mixtures, where multiplying all the scattering lengths by a constant leaves $n^{(0)}a^3_{+1,+1}$ invariant [16].

As it can be seen in Fig. 1, other phases arise as the ground state of the system for high enough values of $\Omega$.

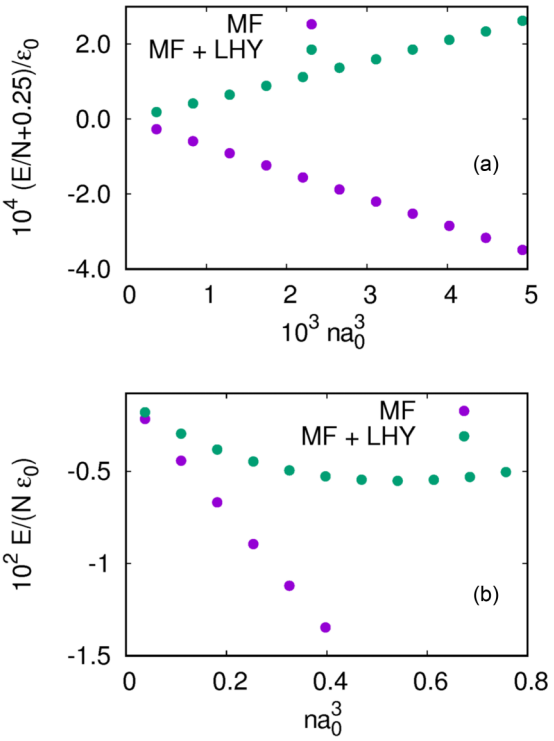


FIG. 2. Rescaled mean field and total energy per particle terms for (a) $\Omega = 2$ and $a_{+1,+1} = 0.1$ and (b) $\Omega = 0.125$ and $a_{+1,+1} = 0.05$. In both cases, $\gamma = -21$.

The plane-wave phase is energetically favorable for $\Omega \gtrsim 3.8$, $a_{+1,+1} \gtrsim 0.1$, and $n > 3.78 \times 10^{-4}$ (although the single minimum phase may have lower energy for high enough densities), while the single minimum phase is the ground state of the system for $\Omega > 4$, $a_{+1,+1} \gtrsim 0.03$, and $n > 3.78 \times 10^{-4}$. Remarkably, the plane-wave and single minimum phases arise only as a gas, while the stripe liquid is present as the ground state of the system for all values of $\Omega$ if $a_{+1,+1} \lesssim 0.025$. This differs from the results obtained for fully repulsive interactions, for which the single minimum phase is the ground state of the system for $\Omega > 4$ both at the mean-field level [5] and when correlations are introduced [15].

The phase diagram of Fig. 1 has been computed by setting $a_{+1,-1} = -1.1a_{+1,+1}$. However, due to the mean-field instability present for $a_{+1,-1} < -a_{+1,+1}$, the LHY correction yields clearly unphysical imaginary contributions to the energy, since the excitation spectrum becomes imaginary at low momenta. In order to avoid that, and as usually done in the non-SOC case, we evaluate the LHY correction for $a_{+1,-1} = -a_{+1,+1}$, i.e., in the limit of the mean-field stability, while the mean-field energy terms are computed for $a_{+1,-1} < -a_{+1,+1}$. The changes in the phase diagram reported in Fig. 1 when $E_{\rm LHY}(a_{+1,-1} = -a_{+1,+1})$ is used instead of $\mathrm{Re}\{E_{\rm LHY}(a_{+1,-1} = -1.1a_{+1,+1})\}$ are accounted for in the error bars.

### C. Extended Gross-Pitaevskii equation and supersolid striped droplets

As it also happens in ultradilute non-SOC Bose-Bose mixtures, a finite-size system in the liquid stripe phase can

form a droplet. However, in the SOC case, the droplets show a striped pattern along the $x$ direction, defined by $\hat{P}_x$ in $\hat{W}^{\mathrm{SOC}}$. Since Raman SOC stripes are known to be supersolid [11,14,15], the resulting striped droplets represent an alternative quantum state of matter that mixes the self-bound character of liquids, the spatial periodicity present in solids, and a superfluid behavior. To obtain the ground state of the finite system, we solve the extended Gross-Pitaevskii equation (EGPE). To this end, we build a density-dependent energy functional by fitting the obtained LHY energy correction for different densities $n$. The chosen functional form is $[E_{\mathrm{LHY}}/N](n) = bn + an^{3/2}$, with $a$ and $b$ two fitting parameters, which consistently reproduces our data in the range of densities spanned in this work. In order to obtain the EGPE, we minimize $E(\Psi, \Psi^\dagger) = \int d\vec{r}\,[\epsilon_{\mathrm{MF}}(\Psi, \Psi^\dagger) + V_{\mathrm{osc}}(\vec{r}\,)|\Psi|^2 + \epsilon_{\mathrm{LHY}}(\Psi, \Psi^\dagger)]$, replacing $n \to \Psi^\dagger\Psi$ in the $\epsilon_{\mathrm{LHY}}$ term. Here $\epsilon_{\mathrm{MF}}$ and $\epsilon_{\mathrm{LHY}}$ are the mean-field and Lee-Huang-Yang energy densities of the infinite system, respectively, and $\Psi$ is the spinor wave function. The harmonic-oscillator potential $V_{\mathrm{osc}}(\vec{r}\,) = \omega^2 r^2$ in reduced units is added to keep the system finite.

Solving directly the EGPE is technically involved for some values of the system size because of the presence of two very different length scales: the period of the stripes, which for values of $\Omega \leqslant 1$ is $L_s \sim O(1)$, and the radius of the droplet, which is generally much larger. Nevertheless, the results for a set of parameters for which the problem is well conditioned show that the spinor ground-state wave function of the system obtained from the EGPE can be well approximated by

$$\Psi^{+1}(\vec{r}\,) = \Psi^{-1}(\vec{r}\,) \simeq f_{\mathrm{stripe}}(x) f_{\mathrm{droplet}}(r), \tag{8}$$

with errors on the momentum of the stripes of at most 5%. Here $f_{\mathrm{stripe}}(x) \simeq \sqrt{\tilde{V}}\psi_0^{\pm 1}(\vec{r}\,)$, a dimensionless factor which equals Eq. (5) multiplied by $\sqrt{\tilde{V}}$ and considering only the $n = -1$ and $n = 0$ terms in the sum. This is equivalent to taking the mean-field ansatz of Ref. [5] divided by $\sqrt{n}$. The function $f_{\mathrm{droplet}}(r)$ depends only on $r = |\vec{r}\,|$, with $\vec{r}$ the position vector in three dimensions. In order to efficiently calculate $f_{\mathrm{droplet}}(r)$, we apply a further approximation by solving the EGPE obtained from the functional $\tilde{E}(\Psi, \Psi^\dagger) = \int d\vec{r}\,[\tilde{\epsilon}_{\mathrm{MF}}(\Psi, \Psi^\dagger) + V_{\mathrm{osc}}(\vec{r}\,)|\Psi|^2 + \epsilon_{\mathrm{LHY,\,SOC}}(\Psi, \Psi^\dagger)]$. Here $\tilde{\epsilon}_{\mathrm{MF}}$ is the mean-field energy density obtained with the SOC terms removed, while $\epsilon_{\mathrm{LHY,SOC}}$ is the LHY energy density obtained from the full SOC calculation. Then the resulting EGPE can be solved efficiently as the problem only depends on $r$.

There is a minimum particle number required to have a stable self-bound droplet in the ground state, which is known as the critical number $N_{\mathrm{crit}}$. We determine $N_{\mathrm{crit}}$ by solving the EGPE for different strengths of the trapping potential and comparing the solution obtained to the ground-state wave function of the harmonic oscillator. For $N \geqslant N_{\mathrm{crit}}$, changing the trapping strength leaves the solution of the EGPE unaffected. We show in Fig. 3 the normalized wave function, obtained under the aforementioned approximations, along the $x$ axis, corresponding to a case where a stable droplet is formed, with the parameters $\Omega = 0.5$, $a_{+1,+1} = 0.12$, $\gamma = -21$, and $N = 1.4 \times 10^5$. The trapping strengths are $\omega_1 = 4.93 \times 10^{-6}$ and $\omega_2 = 2.77 \times 10^{-6}$. We only show the $+1$ spinor component, since $\Psi^{+1}(\vec{r}\,) = \Psi^{-1}(\vec{r}\,)$. We also report the noninteracting harmonic-oscillator ground-state wave function for each one of the trapping frequencies. We do so to showcase the self-bound character of the dropletlike solution: Since the characteristic size of the normalized wave function is much smaller than the characteristic length of the harmonic trap, this indicates that the system is in a self-bound state. As one can also see in Fig. 3, the density profile of the droplet clearly manifests oscillations in the density, characteristic of the stripe phase. Using the units of Ref. [10], one can see that stripes with similar periodicity and contrast such as those shown in Fig. 3 have already been observed experimentally through Bragg scattering [10].

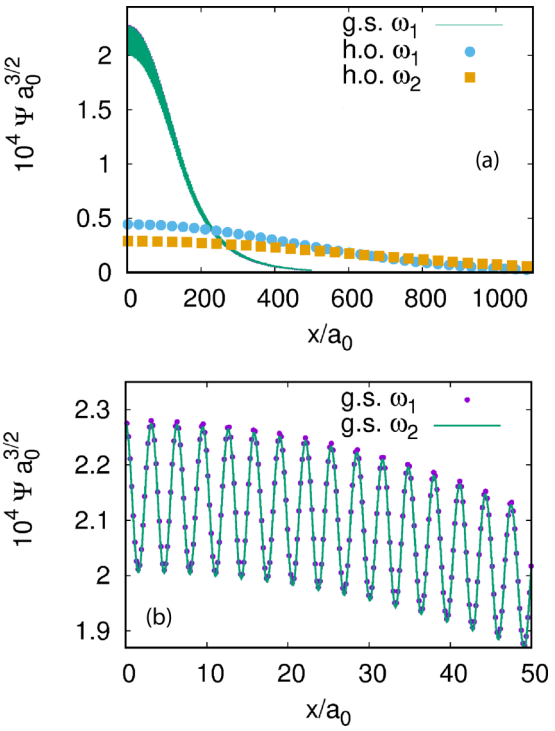


FIG. 3. (a) Normalized wave function of the droplet along the $x$ axis for $\Omega = 0.5$, $a_{+1,+1} = 0.12$, $\gamma = -21$, and $N = 1.4 \times 10^5$ with $\omega_1 = 4.93 \times 10^{-6}$ (green line). The profile corresponding to the same $N$, $a_{+1,+1}$, $\gamma$, and $\Omega$ values but for $\omega_2 = 2.77 \times 10^{-6}$ is indistinguishable from the one reported in (a). The harmonic-oscillator ground-state solution for both values of $\omega$ is shown as squares and circles. (b) Magnified view of the two droplet wave functions at small $x$. Only $x > 0$ values are displayed since the profile is symmetric on the $x$ axis.

We report in Fig. 4 the critical number as a function of $a_{+1,+1}$ for $\Omega = 0.125$, 0.5, and 1.0 and $\gamma = -21$ ($a_{+1,-1} = -1.1a_{+1,+1}$). Error bars account for the numerical inaccuracies associated with both the finite number of Brillouin zones being integrated and the number of points used in the computation of $E_{\mathrm{LHY}}$ and also for the difference in the results obtained when employing either $E_{\mathrm{LHY}}(a_{+1,-1} = -a_{+1,+1})$ or $E_{\mathrm{LHY}}(a_{+1,-1} = -1.1a_{+1,+1})$. As can be seen from the figure, the critical number increases with both $\Omega$ and the scattering lengths, consistently with the results shown in Fig. 1. It must be remarked that, for values of $N$ above the critical numbers listed in Fig. 4, the self-bound droplet corresponds to the ground state of the system. Remarkably, the critical numbers

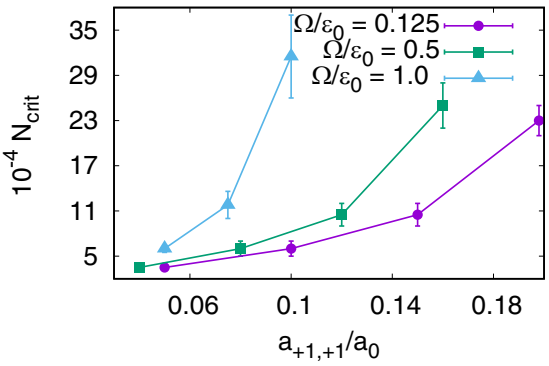


FIG. 4. Critical number as a function of the scattering length $a_{+1,+1}$ for $\gamma = -21$ ($a_{+1,-1} = -1.1a_{+1,+1}$) for different values of $\Omega$. Lines are a guide to the eye.

obtained are reachable in current experimental setups, opening the possibility to observe and measure quantum properties of striped droplets. For the sake of comparison, previous experiments with SOC systems have been carried out with $N \sim 1.8 \times 10^5$ [4] and $N \sim 10^5$ [10] particles. Another interesting quantity regarding the number of particles of a droplet is the saturation number $N_s$. If $N > N_s$, $f_{\text{droplet}}(r)$ shows a plateau at a range of positions $r \in [0, r_{\max}]$, with $r_{\max}$ increasing as $N$ increases. For $\Omega = 0.125$, the saturation number in all cases is of $O(10^6)$ or higher, which makes it challenging to observe.

Despite the evaluation of $E_{\text{LHY}}$ for SOC systems presented in this work being more elaborate than in non-SOC systems, the resulting observed dependence on the system parameters is smooth enough to allow for a simple functional form approximation. In this way, we report an approximated density functional for $E_{\text{LHY}}(a_{+1,-1} = -a_{+1,+1})$ in the stripe phase. This functional depends on $a_{+1,+1}$, $n$, and $\Omega$ and has been obtained by fitting the LHY energies in different density regimes. It is given by

$$E_{\text{LHY}}/N|_{a_{+1,-1}=-a_{+1,+1}} \simeq (A + B\Omega^2) n a_{+1,+1}^2 + C\sqrt{n^3 a_{+1,+1}^5}, \tag{9}$$

with $A = 1.89 \pm 0.04$, $B = 2.17 \pm 0.03$, and $C = 37 \pm 2$ in dimensionless form. The above expression reproduces the obtained LHY energies with errors between 1% and 10% for $0 < \Omega < 3$, $0 < n \lesssim 0.1$, and $0 < a_{+1,+1} < 0.225$, although the limiting value of the density can be increased further for scattering lengths $a_{+1,+1} \lesssim 0.05$, keeping the error of the functional approximation within the mentioned boundaries.

The are several reasons behind the choice of the functional form in Eq. (9). The functional features a difference of one between the exponents of the scattering length and the density in each term, as can be seen from the solution of the Bogoliubov–de Gennes equations. Also, the linear dependence with respect to the density can be clearly observed in low-density regimes. The term proportional to $\sqrt{n^3 a_{+1,+1}^5}$ has been chosen in analogy with the non-SOC case. Finally, the fitting process reveals that higher-order terms with respect to the density and the scattering length are irrelevant in the density regimes considered in this work.

Regarding the potential experimental observation of the ultradilute, supersolid striped droplets, we have performed calculations of the liquid equation of state and the critical number for droplet formation for parameters close to the experimental conditions of Refs. [4,10], $\Omega^{(1,2)} = 0.313$ and $a_{+1,+1}^{(1)} \simeq 0.025$ for the case close to Ref. [10], and $a_{+1,+1}^{(2)} = 0.0146$ for the case close to Ref. [4]. The densities are $n^{(1)} = 5.82$ and $n^{(2)} \simeq 50.2$, with all quantities expressed in reduced units. However, we have set $\gamma = -21$ to enable the formation of droplets, unlike the scattering lengths employed in both experiments, which are positive and thus make the formation of droplets not possible. Remarkably, both experimental systems lie within the stripe liquid region of the diagram of Fig. 1, which implies that an interaction with an attractive enough interspin component should lead to the formation of supersolid striped droplets. Moreover, the minimum of the energy per particle is located at a density close to the one employed in both experiments, with $n_{\min}^{(1)} = 7.1 \pm 1.5$ and $n_{\min}^{(2)} = 40 \pm 10$. Regarding the critical number, it lies below particle numbers employed in both experiments, since $N^{(1)} = 10^5$ and $N^{(2)} = 1.8 \times 10^5$, while we find $N_{\text{crit}}^{(1)} = 22\,500 \pm 2500$ and $N_{\text{crit}}^{(2)} = 17\,500 \pm 2500$. For the particle numbers used in the experiments, the droplets have central densities of $n_{\text{cent}}^{(1)} \simeq 7.9$ and $n_{\text{cent}}^{(2)} \simeq 42.9$. Although our calculations are restricted to the case $a_{+1,+1} = a_{-1,-1}$ and $a_{+1,-1} = -1.1a_{+1,+1}$, both experiments lie far from the liquid-gas transition of Fig. 1 in terms of both $\Omega$ and $a_{+1,+1}$. Therefore, we do not expect the modification of any of the conditions considered in this work regarding the scattering lengths to disable droplet formation under the experimental parameters of Refs. [4,10].

## IV. CONCLUSION

We have evaluated the role of quantum fluctuations in a striped system under Raman SOC that is unstable at the mean-field level. We have found that quantum fluctuations prevent the mean-field collapse as happens in regular ultradilute non-SOC Bose-Bose mixtures. However, the presence of SOC induces the emergence of two stable stripe phases, a gas phase and a liquid phase, with the Raman coupling and the scattering lengths determining the one that is energetically favorable. The stripe liquid phase of this system represents a state of matter which shows superfluidity and periodicity along one direction. We have evaluated the ground state of the finite system by solving the EGPE to find self-bound dropletlike solutions with periodicity along the $x$ axis as a result. These droplets represent a different state of matter that combines the self-bound character of liquids, a density modulation, and superfluidity. We have also computed the critical numbers associated with the self-bound droplet states and found that they are experimentally accessible. Finally, we have provided an approximated energy functional for the Lee-Huang-Yang energy in the stripe phase. We hope that this work can inspire new experiments to detect the proposed supersolid striped droplets.

## ACKNOWLEDGMENTS

We acknowledge L. Tarruell and V. Cikojević for fruitful discussions. This work was supported by MINECO (Spain)

Grant No. FIS2017-84114-C2-1-P. J.S.-B. also acknowledges support from an FPU Fellowship through Grant No. FPU15/01805 from MCIU.

## APPENDIX A: APPROXIMATIONS ON THE NUMERICAL COMPUTATION OF THE LEE-HUANG-YANG INTEGRAL

The unregularized Lee-Huang-Yang energy per particle is given by

$$E_{\mathrm{LHY}}^{\mathrm{unreg}}/N = \frac{1}{n}(I_1 + I_2 + I_3), \tag{A1}$$

$$I_1 = \sum_{\substack{l,l' \\ s_1,s_2}} \frac{1}{(2\pi)^3} \int_{\substack{0<k_x<k_1 \\ 0<k_y,\,k_z<\infty}} d\vec{k}\Big\{f_{\vec{k}_1-\vec{k},l,l',s_1} f^*_{\vec{k}_1-\vec{k},l,l',s_2}\big[H_0\big(\vec{k}_1+\vec{k}+2l'\vec{k}_1,s_1,s_2\big)-\delta_{s_1,s_2}\mu\big]$$

$$+g_{\vec{k}_1+\vec{k},l,l',s_1} g^*_{\vec{k}_1+\vec{k},l,l',s_2}\big[H_0(\vec{k}_1-\vec{k}+2l'\vec{k}_1,s_1,s_2)-\delta_{s_1,s_2}\mu\big]\Big\}, \tag{A2}$$

$$I_2 = \frac{8\pi n}{(2\pi)^3} \sum_{\substack{l \\ n_1,n_2,n_3,n_4 \\ s_1,s_2}} \int_{\substack{0<k_x<k_1 \\ 0<k_y,\,k_z<\infty}} d\vec{k}\big[\psi^*_{0,n_1,s_1}\psi^*_{0,n_2,s_2}a_{s_1,s_2}$$

$$\times\big(g^*_{\vec{k}_1+\vec{k},l,n_3,s_1} f_{\vec{k}_1+\vec{k},l,n_4,s_2} + f^*_{\vec{k}_1-\vec{k},l,n_3,s_1} g_{\vec{k}_1-\vec{k},l,n_4,s_2}\big)\delta(n_3+n_4-n_1-n_2)\big], \tag{A3}$$

$$I_3 = \frac{8\pi n}{(2\pi)^3} \sum_{\substack{l \\ n_1,n_2,n_3,n_4 \\ s_1,s_2}} \int_{\substack{0<k_x<k_1 \\ 0<k_y,\,k_z<\infty}} d\vec{k}\big[\psi^*_{0,n_1,s_1}\psi_{0,n_2,s_1}a_{s_1,s_2}\big(g_{\vec{k}_1+\vec{k},l,n_3,s_2} g^*_{\vec{k}_1+\vec{k},l,n_4,s_2} + f^*_{\vec{k}_1-\vec{k},l,n_3,s_2} f_{\vec{k}_1-\vec{k},l,n_4,s_2}\big)$$

$$\times\,\delta(-n_3+n_4-n_1+n_2) + \psi^*_{0,n_1,s_1}\psi_{0,n_2,s_2}a_{s_1,s_2}\big(g_{\vec{k}_1+\vec{k},l,n_3,s_1} g^*_{\vec{k}_1+\vec{k},l,n_4,s_2} + f^*_{\vec{k}_1-\vec{k},l,n_3,s_1} f_{\vec{k}_1-\vec{k},l,n_4,s_2}\big)$$

$$\times\,\delta(-n_3+n_4-n_1+n_2)\big], \tag{A4}$$

where $s_1$ and $s_2$ are spinor component indices, $\mu$ is the chemical potential, $n$ is the density, and we have expanded the Bogoliubov amplitudes of Eq. (7) in Bloch waves [20]

$$\vec{f}_{\vec{k}_1+\vec{k},l}(\vec{k},\vec{r}\,) = \frac{1}{\sqrt{\tilde{V}}} e^{i(\vec{k}_1+\vec{k})\vec{r}} \sum_{n\in\mathbb{Z}} \vec{f}_{\vec{k}_1+\vec{k},l,n} e^{2ink_1x}, \tag{A5}$$

$$\vec{f}^*_{\vec{k}_1-\vec{k},l}(\vec{k},\vec{r}\,) = \frac{1}{\sqrt{\tilde{V}}} e^{i(\vec{k}_1+\vec{k})\vec{r}} \sum_{n\in\mathbb{Z}} \vec{f}^*_{\vec{k}_1-\vec{k},l,n} e^{2ink_1x}, \tag{A6}$$

$$\vec{g}_{\vec{k}_1-\vec{k},l}(\vec{k},\vec{r}\,) = \frac{1}{\sqrt{\tilde{V}}} e^{i(\vec{k}_1-\vec{k})\vec{r}} \sum_{n\in\mathbb{Z}} \vec{g}_{\vec{k}_1-\vec{k},l,n} e^{2ink_1x}, \tag{A7}$$

$$\vec{g}^*_{\vec{k}_1+\vec{k},l}(\vec{k},\vec{r}\,) = \frac{1}{\sqrt{\tilde{V}}} e^{i(\vec{k}_1-\vec{k})\vec{r}} \sum_{n\in\mathbb{Z}} \vec{g}^*_{\vec{k}_1+\vec{k},l,n} e^{2ink_1x}, \tag{A8}$$

with $\vec{f}_{\vec{k},l,n} = (f_{\vec{k},l,n,s=+1} f_{\vec{k},l,n,s=-1})^\tau$. The same holds for $\vec{g}_{\vec{k},l,n}$. The terms $\psi_{0,n,s}$ correspond to the expansion in Bloch waves of the condensate wave function (see the main text). The integration region in Eqs. (A2)–(A4) is $k_\perp = \sqrt{k_y^2+k_z^2} \in [0,\infty)$, $0 < k_x < k_1$, with $k_1$ the ground-state momentum. The sum indices $\{l, n_1, n_2, n_3, n_4\}$ range from $-\infty$ to $+\infty$. In practice, we introduce cutoff values in both operations and restrict the calculation to $0 < k_\perp = \sqrt{k_y^2+k_z^2} < k_{\perp,\max}$ and $-N_c < l, n_1, n_2, n_3, n_4 < N_c - 1$. The integration volume is then $V_I = \pi k_{\perp,\max}^2 \times 4N_c k_1$, a cylinder of radius $k_{\perp,\max}$ in the $\{k_y, k_z\}$ plane and height $4N_c k_1$ in the $k_x$ axis, centered at the origin. The Bloch amplitudes fulfill the normalization condition [20]

$$\sum_{n=-N_c}^{n=N_c-1} \vec{f}^{\,\tau}_{k_1+\vec{k},l,n}\vec{f}_{k_1+\vec{k},l,n} - \big(\vec{g}^{\,\tau}_{k_1+\vec{k},l,n}\vec{g}_{k_1+\vec{k},l,n}\big) = 1, \tag{A9}$$

$$\sum_{n=-N_c}^{n=N_c-1} \vec{f}^{\,\tau}_{k_1-\vec{k},l,n}\vec{f}_{k_1-\vec{k},l,n} - \big(\vec{g}^{\,\tau}_{k_1-\vec{k},l,n}\vec{g}_{k_1-\vec{k},l,n}\big) = -1. \tag{A10}$$

We define $N_x$ and $N_\perp$ as the number of points on the $x$ and radial axes, respectively. Looking at Eq. (A1), one notices that the integral scales as $O(N_x N_\perp N_c^4)$, while typically $N_x \sim O(10^2)$, $N_\perp \sim O(10^3)$, and the calculation becomes too expensive in computational cost terms. In order to make it feasible, we introduce two approximations. The first one involves the number of momentum components of the condensate wave function [i.e., indices $n_1$ and $n_2$ in Eq. (A1)]. According to Ref. [20] and to our simulated-annealing calculations, the absolute value of the Bloch wave amplitudes in the condensate wave function decreases very rapidly with the momentum index, $n$. Therefore, we denote by $N_{c,0}$ the number of momentum components of the condensate wave function included in the computation of the LHY integral and set its value. In this way, the LHY integral scales as $O(N_x N_\perp N_{c,0}^2 N_c^2)$, with the integration volume remaining unchanged. In practice, no significant changes are seen in the results when $N_{c,0} > 5$, so we set $N_{c,0} = 5$.

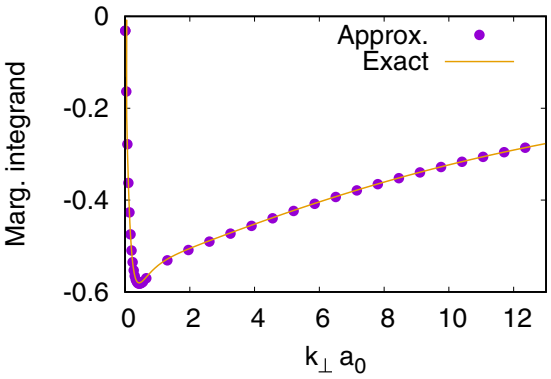


FIG. 5. Exact ($N_c = 9$) and approximated ($N_c = 9$ and $N_{c,0} = 5$) marginal integrands of the unregularized LHY energy per particle for $\Omega = 2.8$, $a_{+1,+1} = a_{-1,-1} = 0.641\,982$, $\gamma = 0.4$, $n = 3.7 \times 10^{-3}$, $N_x = 200$, and $N_\perp = 2000$.

The computation cost can be further reduced by introducing a second approximation. It can be checked numerically that, as $k_\perp$ and $N_c$ increase, the integral $I_2$ is dominated by the contributions from the $f_{\vec{k}_1+\vec{k},l,l,\pm1}$ and $g_{\vec{k}_1-\vec{k},l,l,\pm1}$ terms. Therefore, we retain the two dominant terms for every value of $l$ to the integral instead of performing the whole sum over $n_3$ and $n_4$. Additionally, we retain only the two first momentum modes of the condensate state when computing the integral $I_3$, since we have checked that these are the dominant contributions. These approximations reduce the scaling of the LHY integral on $N_c$ up to $\max\{O(N_x N_\perp N_c N_{c0}^2), O(N_x N_\perp N_c^2)\}$. We show in Fig. 5 the marginal integrand of $E_{\rm LHY}/N$ after integrating over the $x$ axis and performing the sums, for the exact case with $N_c = 9$ and the approximated case with $N_c = 9$ and $N_{c,0} = 5$. As it can be seen from the figure, both curves are in excellent agreement.

## APPENDIX B: REGULARIZATION OF THE LHY INTEGRAL

We define $\epsilon_{\rm LHY}(V_I)$ as the integral of Eq. (A1) over a finite integration volume $V_I$. As mentioned in the main text,

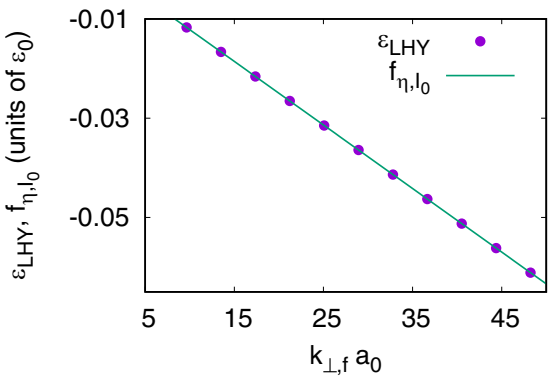


FIG. 6. Plot of $\epsilon_{\rm LHY}$ (blue circles) and $f_{\eta,I_0}$ (green line) computed for different integration volumes $V_I$, with $V_I = \pi k_{\perp,\rm f}^2 \times 2k_{\perp,\rm f}$, a cylinder of radius $k_{\perp,\rm f}$, and height $2k_{\perp,\rm f}$, with $k_{\perp,\rm f} = 2N_c k_1$, $N_c \in [5, 25]$. The other parameters are $\Omega = 1.0$, $a_{+1,+1} = a_{-1,-1} = 0.2$, $\gamma = -21$, $n = 3.11 \times 10^{-3}$, $N_x = 300$, and $N_\perp = 3000$.

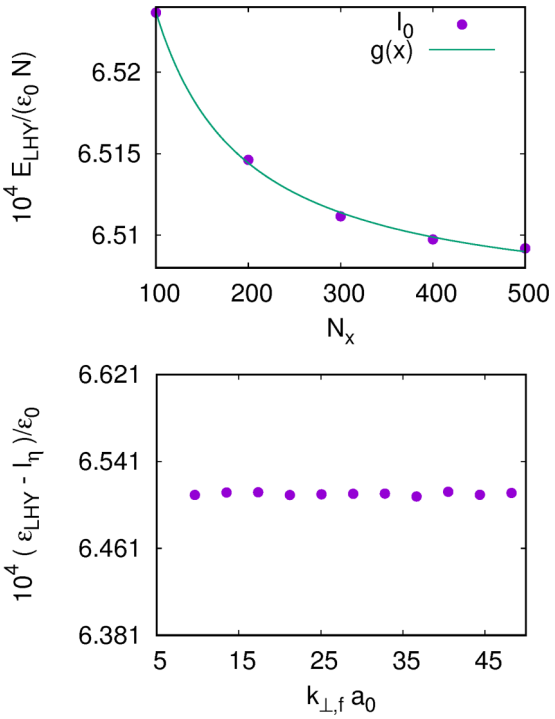


FIG. 7. (a) Plot of $I_0(N_x)$ vs $N_x$. (b) Plot of $\epsilon_{\rm LHY}(V_I) - I_\eta(V_I)$ computed for different integration volumes $V_I$, with $V_I = \pi k_{\perp,\rm f}^2 \times 2k_{\perp,\rm f}$, a cylinder of radius $k_{\perp,\rm f}$, and height $2k_{\perp,\rm f}$. The other parameters are $\Omega = 1.0$, $a_{+1,+1} = a_{-1,-1} = 0.2$, $\gamma = -21$, and $n = 3.11 \times 10^{-3}$.

the LHY integral for a Raman SOC stripe system is ultraviolet divergent [i.e., $\lim_{V_I\to\infty} \epsilon_{\rm LHY}(V_I) = \infty$] and must be regularized. To identify the diverging behavior, we compute $\epsilon_{\rm LHY}(V_I)$ over increasingly larger cylindrical volumes. These volumes are defined as $V_I^{(i)} = \pi (k_{\perp,\max}^{(i)})^2 \times 4N_c^{(i)} k_1$, with $k_{\perp,\max}^{(i)} = 2N_c^{(i)} k_1$, $N_c^{(i)} \in \mathbb{N}$. We find that $\epsilon_{\rm LHY}(V_I)$ can be fitted to

$$f_{\eta,I_0}(V_I) = \int_{V_I} d\vec{k}\, \eta/k^2 + I_0 = I_\eta(V_I) + I_0, \tag{B1}$$

with $\eta$ and $I_0$ fitting parameters, $k^2 = k_x^2 + k_y^2 + k_z^2$, and $I_\eta(V_I)$ given by

$$I_\eta(V_I) = 8\pi\eta N_c k_1 \left(\frac{\pi}{4} + \frac{\ln 2}{2}\right), \tag{B2}$$

where ln indicates the natural logarithm. We show $\epsilon_{\rm LHY}(V_I)$ and $f_{\eta,I_0}(V_I)$ as a function of the integration volume in Fig. 6. Therefore, the quantity $\lim_{V_I\to\infty} \epsilon_{\rm LHY}(V_I) - I_\eta(V_I)$ is finite. Thus, the LHY energy per particle can be computed as

$$E_{\rm LHY}/N = \lim_{V_I\to\infty} [\epsilon_{\rm LHY}(V_I) - I_\eta(V_I)] + I_\eta^{\rm reg}, \tag{B3}$$

with $I_\eta^{\rm reg}$ the regularized $I_\eta(\infty)$ value, which we obtain by applying dimensional regularization [22,23]. In this scheme, the regularized integral of a polynomial identically vanishes [22], which implies $I_\eta^{\rm reg}(V_I = \infty) = 0$. Thus, the regularized LHY integral is given by

$$E_{\rm LHY}/N = \lim_{V_I\to\infty} [\epsilon_{\rm LHY}(V_I) - I_\eta(V_I)] = I_0. \tag{B4}$$

## APPENDIX C: CONVERGENCE OF THE REGULARIZED LHY INTEGRAL

Ideally, the regularized LHY integral should be computed for $N_c \to \infty$, $N_x \to \infty$, and $N_\perp \to \infty$. However, in practice, the values $N_c$, $N_x$, and $N_\perp$ used in the calculations are finite. In order to approach the asymptotic limit, the regularized LHY integral is computed for different values $N_c \in [n_{c,0}, n_{c,1}]$ and for a different number of points $N_x \in [n_{x,0}, n_{x,1}]$, with $N_\perp = 10N_x$. For each value of $N_c$, the cylindrical integration volume is $V_I = \pi(2N_c k_1)^2 \times 4N_c k_1$, analogously to Appendix B. For each fixed number of points, the fitting described in Appendix B is carried out, resulting in a function $I_0(N_x)$. We then extrapolate $I_0(N_x)$ to $N_x \to \infty$ using a function of the form $g(N_x) = a + b/N_x^l$ and take the extrapolation $I_0(N_x \to \infty)$ as the final result. The range of $N_c$ is chosen such that the quantity $\epsilon_{\rm LHY}(V_I) - I_\eta(V_I)$ does not depend on $N_c$, meaning that the asymptotic limit has been reached. We show in Fig. 7 $I_0(N_x)$ as a function of the number of points $N_x$ for $\Omega = 1.0$, $a_{+1,+1} = a_{-1,-1} = 0.2$, $\gamma = -21$, $n = 3.11 \times 10^{-3}$, and the quantity $\epsilon_{\rm LHY}(V_I) - I_\eta(V_I)$ as a function of the number of modes $N_c$, for $N_x = 300$. As it can be seen from the figure, $\epsilon_{\rm LHY}(V_I) - I_\eta(V_I)$ shows no significant dependence on $N_c$. The extrapolation of $I_0(N_x)$ to $N_x \to \infty$ yields the final result $E_{\rm LHY}/N = I_0(N_x \to \infty) = 6.505 \times 10^{-4}$. In practice, one can just perform the calculations for two values of $N_c$ and one for $N_x$ such that $I(N_x) \simeq I(N_x \to \infty)$. As an example, setting $N_c = 5, 7$ and $N_x = 600$, one obtains $E_{\rm LHY}/N = I_0(N_x = 600) = 6.494 \times 10^{-4} \simeq I_0(N_x \to \infty)$.


[1] M. Z. Hasan and C. L. Kane, Rev. Mod. Phys. **82**, 3045 (2010).

[2] M. Sato and Y. Ando, Rep. Prog. Phys. **80**, 076501 (2017).

[3] L. Zhang and X.-J. Liu, *in Synthetic Spin-Orbit Coupling in Cold Atoms*, edited by W. Zhang, W. Yi, and C. A. R. Sá de Melo (World Scientific, Singapore, 2018), pp. 1–87.

[4] Y.-J. Lin, K. Jiménez-García, and I. B. Spielman, Nature (London) **471**, 83 (2011).

[5] Y. Li, L. P. Pitaevskii, and S. Stringari, Phys. Rev. Lett. **108**, 225301 (2012).

[6] C. Hamner, Y. Zhang, M. A. Khamehchi, M. J. Davis, and P. Engels, Phys. Rev. Lett. **114**, 070401 (2015).

[7] T. M. Bersano, J. Hou, S. Mossman, V. Gokhroo, X.-W. Luo, K. Sun, C. Zhang, and P. Engels, Phys. Rev. A **99**, 051602(R) (2019).

[8] L. W. Cheuk, A. T. Sommer, Z. Hadzibabic, T. Yefsah, W. S. Bakr, and M. W. Zwierlein, Phys. Rev. Lett. **109**, 095302 (2012).

[9] P. Wang, Z.-Q. Yu, Z. Fu, J. Miao, L. Huang, S. Chai, H. Zhai, and J. Zhang, Phys. Rev. Lett. **109**, 095301 (2012).

[10] J.-R. Li, J. Lee, W. Huang, S. Burchesky, B. Shteynas, F. Ç. Top, A. O. Jamison, and W. Ketterle, Nature (London) **543**, 91 (2017).

[11] Y. Li, G. I. Martone, L. P. Pitaevskii, and S. Stringari, Phys. Rev. Lett. **110**, 235302 (2013).

[12] A. Macia, J. Boronat, and F. Mazzanti, Phys. Rev. A **90**, 061601(R) (2014).

[13] R. Bombin, J. Boronat, and F. Mazzanti, Phys. Rev. Lett. **119**, 250402 (2017).

[14] X.-L. Chen, J. Wang, Y. Li, X.-J. Liu, and H. Hu, Phys. Rev. A **98**, 013614 (2018).

[15] J. Sánchez-Baena, J. Boronat, and F. Mazzanti, Phys. Rev. A **101**, 043602 (2020).

[16] D. S. Petrov, Phys. Rev. Lett. **115**, 155302 (2015).

[17] C. R. Cabrera, L. Tanzi, J. Sanz, B. Naylor, P. Thomas, P. Cheiney, and L. Tarruell, Science **359**, 301 (2018).

[18] G. Semeghini, G. Ferioli, L. Masi, C. Mazzinghi, L. Wolswijk, F. Minardi, M. Modugno, G. Modugno, M. Inguscio, and M. Fattori, Phys. Rev. Lett. **120**, 235301 (2018).

[19] G. I. Martone, Y. Li, L. P. Pitaevskii, and S. Stringari, Phys. Rev. A **86**, 063621 (2012).

[20] G. I. Martone and G. V. Shlyapnikov, J. Exp. Theor. Phys. **127**, 865 (2018).

[21] J. R. Harland and P. Salamon, Nucl. Phys. B **5**, 109 (1988).

[22] L. Salasnich and F. Toigo, Phys. Rep. **640**, 1 (2016).

[23] G. Leibbrandt, Rev. Mod. Phys. **47**, 849 (1975).